An ab Initio Study of Nucleophilic Attack of Trimethyl Phosphate: Factors Influencing Site Reactivity

Nai-yuan Chang[†] and Carmay Lim*[,†,‡]

Institute of Biomedical Sciences, Academia Sinica, Taipei, Taiwan 11529, and Department of Chemistry, National Tsing-Hua University, Hsin Chu, Taiwan

Received: June 6, 1997; In Final Form: August 19, 1997[⊗]

The reactions of trimethyl phosphate (TMP) have been studied extensively both in the gas phase and in solution. To complement the experimental studies and to gain insight into the factors influencing the site of reactivity, which can be either the carbon atom or phosphorus atom of TMP, we have carried out ab initio calculations to map out the gas-phase activation free energy profiles of the reactions of TMP with three anions, viz., $(OH)^-$, $(CH_3O)^-$, and F^-. The calculations reveal a novel activation free energy pathway for $(OH)^-$ attack of TMP in the gas phase: namely, nucleophilic addition at phosphorus, followed by pseudorotation and subsequent elimination with *simultaneous intramolecular proton transfer*. For the reaction of $(OH)^-$ with TMP at 298 K, nucleophilic substitution reaction at phosphorus is found to be competitive with and slightly faster than S_N2 reaction at carbon. Both reactions yield the same products, $(DMP)^-$ and MeOH, consistent with the products observed experimentally. In the case of $(OH)^-$ and $(CH_3O)^-$, entropy plays a significant role in addition to enthalpy in determining the site of reactivity of TMP in the gas phase; specifically, temperature-independent electrostatic forces favor attack at phosphorus, whereas temperature-dependent entropic factors bias attack toward carbon. Experiments are suggested to test the theoretical predictions.

Introduction

The reactions of trimethyl phosphate (TMP) have been investigated extensively both in the gas phase[1−3] and in solution.[4−8] In gas-phase studies of nucleophilic attack of TMP, the reactant anion (A^-) can attack at carbon displacing dimethyl phosphate anion $(DMP)^-$ (reaction 1) or attack at phosphorus leading to transesterification (reaction 2).

$$A^- + OP(OCH_3)_3 \rightarrow O_2P(OCH_3)_2^- + CH_3A \qquad (1)$$

$$A^- + OP(OCH_3)_3 \rightarrow OP(A)(OCH_3)_2 + CH_3O^- \qquad (2)$$

Hodges *et al.*[2] and Lum and Grabowski[3] have studied the gas-phase reactions of several anions with TMP using the ion cyclotron resonance and flowing afterglow techniques, respectively. They found products arising from substitution at carbon for all anions that displayed bimolecular reaction pathways and concluded that "anion reaction at phosphorus is completely unimportant, being found as a trace product for the oxygen-centered nucleophiles only".[3] This behavior is in stark contrast to the reactivity of TMP in aqueous solution[4−6] and, more generally, the reactions of phosphates in enzymes.[9] Lum and Grabowski[3] suggested that nucleophilic substitution at carbon is kinetically more favorable than nucleophilic substitution at phosphorus as the former produces a much better leaving group than the latter; in other words, $(DMP)^-$ anion is a much better leaving group than methoxide.

For the gas-phase reaction of hydroxide with TMP, nucleophilic substitutions at the carbon and phosphorus sites are expected to yield the same products. However, on the basis of the observation of $(DMP)^-$ as the major product, both Hodges *et al.*[2] and Lum and Grabowski[3] concluded that in the gas phase, hydroxide reacts with TMP principally[2] or almost exclusively[3] at carbon. In our previous studies of methyl ethylene phosphate,[10−12] the orientation of the hydroxyl group relative to the departing oxygen was found to be important in determining the lowest activation free energy pathway for endocyclic cleavage relative to exocyclic cleavage. In this case, the exocyclic cleavage products are ethylene phosphate anion and methanol; i.e., the departing methoxyl group abstracts a proton from an equatorial hydroxyl group of a pentacoordinate intermediate to generate CH_3OH instead of methoxide.[10,11] These results suggest that an analogous pathway could be favorable for the gas-phase $(OH)^-$ attack at the phosphorus atom of TMP.

Due to the ambiguity in the site of nucleophilic attack, which may be the phosphorus or the carbon, ab initio calculations have been carried out to map out the gas-phase activation free energy profiles for the reaction of $(OH)^-$ with TMP. The gas-phase reaction profiles for F^- and $(CH_3O)^-$ attack of TMP were also obtained to provide results for further calibration against experimental data. The gas-phase studies are valuable not only in clarifying the intrinsic site reactivity of TMP but also in decomposing the various factors governing phospho-ester reactivity into intrinsic molecular and environmental components (e.g., due to solvent). In particular, the gas-phase $(OH)^-$ + TMP reaction profiles provide a crucial starting point in mapping corresponding solution free-energy profiles. Details of the calculations are described in the Methods section. The reaction mechanism and activation free energies of the three reactions studied are presented in the Results section. In the Discussion, the reliability of the theoretical results are assessed and the results are compared against known experimental data; the factors influencing the intrinsic reactivity of carbon vs phosphorus sites of TMP with the three nucleophiles are discussed, and experiments are suggested to verify the predictions of theory.

Methods

The gas-phase reaction profiles were initially explored using the Gaussian 94 program[13] at the Hartree−Fock (HF) level with a 6-31+G* basis set, unless stated otherwise. The nature of each transition state was verified by a single imaginary frequency and an intrinsic reaction coordinate[14−16] calculation leading to the expected ground state and products. The

[†] National Tsing-Hua University.
[‡] Academia Sinica.
[⊗] Abstract published in *Advance ACS Abstracts,* October 1, 1997.

S1089-5639(97)01861-6 CCC: $14.00

TABLE 1: Absolute Energies and Entropies of Reactants and Products at 298 K

species	E_{MP2}, hartrees	ZPE,[a] kcal/mol	E_{TRV},[b] kcal/mol	S_{TRV},[c] cal/mol/K
		Reactants		
$(OH)^-$ [d]	−75.587 78	5.67	7.16	41.11
F^- [e]	−99.623 85	0.00	0.89	34.77
$(CH_3O)^-$ [e]	−114.742 73	24.30	26.12	55.04
$(CH_3O)^-$ [d]	−114.743 62	24.21	26.02	54.80
TMP[e]	−760.326 75	90.27	96.90	101.81
TMP[d]	−760.329 16	91.04	97.54	100.68
		Products		
CH_3OH[d]	−115.356 49	34.63	36.69	56.64
ether[d]	−154.513 07	53.93	56.58	62.77
$(DMP)^-$ [d]	−720.652 18	63.54	68.69	90.06
HDMP[d]	−721.176 13	71.70	77.26	92.54
FDMP[e]	−745.173 21	63.29	68.71	92.77

[a] Zero-point energy. [b] $E_{TRV} = E_{trans} + E_{rot} + E_{vib}$. [c] $S_{TRV} = S_{trans} + S_{rot} + S_{vib}$. [d] Single-point MP2/6-31+G* energy calculation at HF/6-31+G* geometry. [e] Single-point MP2/6-31+G* energy calculation at HF/3-21+G* geometry.

TABLE 2: Relative Energies, Entropies, and Free Energies for Reactions of $(OH)^-$, $(CH_3O)^-$, and F^- with TMP at 298 K

species	ΔE[a]	ΔZPE[b]	ΔE_{TRV}[c]	$T\Delta S_{TRV}$[d]	ΔG[e]
		OH^- + TMP			
TMP + $(OH)^-$	0.00	0.00	0.00	0.00	0.00
I-2a	−36.13	3.38	2.32	−11.76	−19.28
I-2b	−37.27	3.27	2.27	−11.59	−20.73
I-2c	−34.11	3.05	2.17	−11.05	−18.44
I-4a	−43.70	3.58	2.51	−11.87	−26.34
I-4b	−39.84	3.25	2.33	−11.43	−23.43
TS-1	−13.32	0.25	0.37	−7.96	−5.34
TS-2	−20.11	1.78	1.08	−10.94	−6.92
TS-Ra	−33.44	2.95	1.54	−12.65	−16.90
TS-Rb	−31.95	2.87	1.50	−12.61	−15.57
TS-3	−21.15	1.29	0.63	−10.64	−9.19
TS-4	−37.60	3.32	1.74	−13.29	−19.86
TS-Rc	−37.06	2.88	1.59	−12.19	−20.99
TS-5	−38.48	2.52	1.44	−11.54	−23.58
$(DMP)^-$ + CH_3OH	−57.55	1.46	0.68	1.46	−56.88
HDMP + $(CH_3O)^-$	−1.76	−0.80	−1.42	1.65	−5.63
		CH_3O^- + TMP			
TMP + $(CH_3O)^-$	0.00	0.00	0.00	0.00	0.00
TS-6	−13.11	0.39	1.10	−8.65	−3.56
TS-7	−18.74	1.89	1.76	−12.58	−3.10
$(DMP)^-$ + CH_3OCH_3	−58.03	2.22	1.71	−0.79	−53.31
		F^- + TMP			
TMP + F^-	0.00	0.00	0.00	0.00	0.00
TS-8	−10.80	−0.39	0.57	3.23	−14.44
TS-9	−17.03	0.83	1.06	0.19	−15.92
TS-10	−3.86	−1.31	−0.63	2.10	−8.50
FDMP + $(CH_3O)^-$	21.75	−2.69	−2.08	13.72	3.26

[a] For the reaction of TMP with $(OH)^-$ and $(CH_3O)^-$, the total electronic energies correspond to single-point MP2/6-31+G* energies at HF/6-31+G* geometry while for F^- + TMP the values correspond to single-point MP2/6-31+G* energies at HF/3-21+G* geometry. Energy in kcal/mol relative to reactants separated at infinity. [b] Zero-point (ZPE) in kcal/mol relative to reactants. [c] $E_{trans} + E_{rot} + E_{vib}$ in kcal/mol relative to reactants. [d] $T^*(S_{trans} + S_{rot} + S_{vib})$ in kcal/mol relative to reactants. [e] $\Delta G = \Delta E + \Delta ZPE = \Delta E_{TRV} + \Delta PV - T\Delta S_{TRV}$.

correlation energy is estimated with second-order Møller−Plesset theory and the 6-31+G* basis set using fully optimized HF/6-31+G* geometries. To assess the reliability of the MP2/6-31+G*//HF/6-31+G* calculations, certain transition states were reoptimized at the MP2/6-31+G* level and the correlation energy was computed using increasing basis sets and levels of theory (see Discussion). The frozen-core approximation (rather than all electrons) was employed in all MP2 correlation calculations.

To determine the thermodynamic parameters, vibrational frequencies were computed for the fully optimized structures of the stationary points along the reaction profile. The HF/6-31+G* frequencies were scaled by an empirical factor of 0.8929 to correct for any errors that may arise from anharmonicity in the potential energy surface, inadequate basis sets, and the neglect of electron correlation.[17] The entropy (S_{vib}), zero-point energy (ZPE), and vibrational energy (E_{vib}) were calculated from the frequencies and geometries according to standard statistical mechanical formulas.[18] The rotational (E_{rot}) and translational (E_{trans}) energies and the work term (PV) were treated classically. Addition of the energetic and entropic corrections to the MP2/6-31+G*//HF/6-31+G* activation energies gave the gas-phase free energy barriers at 298 K.

Results

Schemes 1, 2, and 3 summarize the calculated gas-phase reaction mechanisms for the nucleophilic addition of $(OH)^-$, $(CH_3O)^-$, and F^- to TMP, respectively. The gas-phase free-energy profiles for the three reactions are illustrated in Figures 1−3 and the corresponding thermodynamic data are collected in Tables 1 and 2. In Table 2, the zero of energy corresponds to the reactants at infinite separation. The notation TMP(P) refers to nucleophilic attack at the phosphorus atom of TMP.

OH^- + TMP. Scheme 1 shows that there are three possible pathways following the initial formation of a long-range ion−dipole complex **I-1**. Pathway a is $(OH)^-$ attack at carbon via a S_N2 transition state (**TS-1**) to generate CH_3OH and $(DMP)^-$; the reaction is exothermic with a free energy of −57 kcal/mol.

Pathways b and c proceed via a long-range transition state (**TS-2**), which is formed at a $P-O^H$ distance of 2.56 Å. The **TS-2** transition state has a distorted trigonal-bipyramidal (TBP) geometry with average O(axial)−P−Y, O^H−P−Y, and Y−P−Y (Y = O or O^{Me} equatorial atoms) angles of 99°, 81°, and 118°, respectively. A stable pentacovalent TBP intermediate (**I-2a**) is formed, characterized by C(equatorial)−O−P−O^H dihedral angles of (−28°, 20°) (Figure 4). Rotation of one or both equatorial methoxy group(s) about the P−O(Me) bond yields a lower-energy intermediate (**I-2b**) and a higher-energy intermediate (**I-2c**) characterized by C(equatorial)−O−P−O^H dihedral angles of (−24°, 174°) and (−158°, −159°), respectively (Table 2 and Figure 4). In analogy to the reversal of $(OH)^-$ attack, the lowest energy pathway for elimination of methoxide stems from the **I-2c** intermediate with both equatorial O−C(Me) bonds cis with respect to the scissile P−O(Me) axial bond. Methoxide elimination via **TS-3** leads to another ion−dipole complex, $(CH_3O)^-$...$(HO)(CH_3O)_2PO$ (**I-3**) (Scheme 1), which can yield three different sets of products: (i) $(CH_3O)^-$ and hydrogen dimethyl phosphate, HDMP, via direct dissociation of $(CH_3O)^-$; (ii) CH_3OH and $(DMP)^-$ via *inter*molecular proton transfer, and (iii) CH_3OCH_3 and $((HO)(CH_3O)PO_2)^-$ via nucleophilic substitution at carbon.

Alternatively, the three **I-2** intermediates with the hydroxyl group axial can undergo pseudorotation to form **I-4a** and **I-4b** with the hydroxyl group now in an equatorial position (Figure 4). The **I-4b** intermediate with both equatorial O−H and O−C bonds cis to the P−O bond of an axial methoxy group is destabilized (by 2.9 kcal/mol in free energy) relative to the **I-4a** intermediate, where the O−H bond is cis but the equatorial O−C bond is trans to an axial P−O bond. Both **I-4a** and **I-4b** intermediates can undergo cleavage of the axial P−O bond that is cis to O−H with simultaneous proton transfer via **TS-5** to yield CH_3OH and $(DMP)^-$ (pathway c); however, **I-4b** yields a lower energy pathway than **I-4a**.

The computed reaction mechanisms in Scheme 1 rule out an S_N2 reaction at phosphorus since stable pentacovalent TBP intermediates are found (see Scheme 1 and Figure 4). The

SCHEME 1: Computed $(OH)^-$ + TMP Reaction Pathways Occurring at Carbon (Pathway a) and at Phosphorus (Pathways b and c)[a]

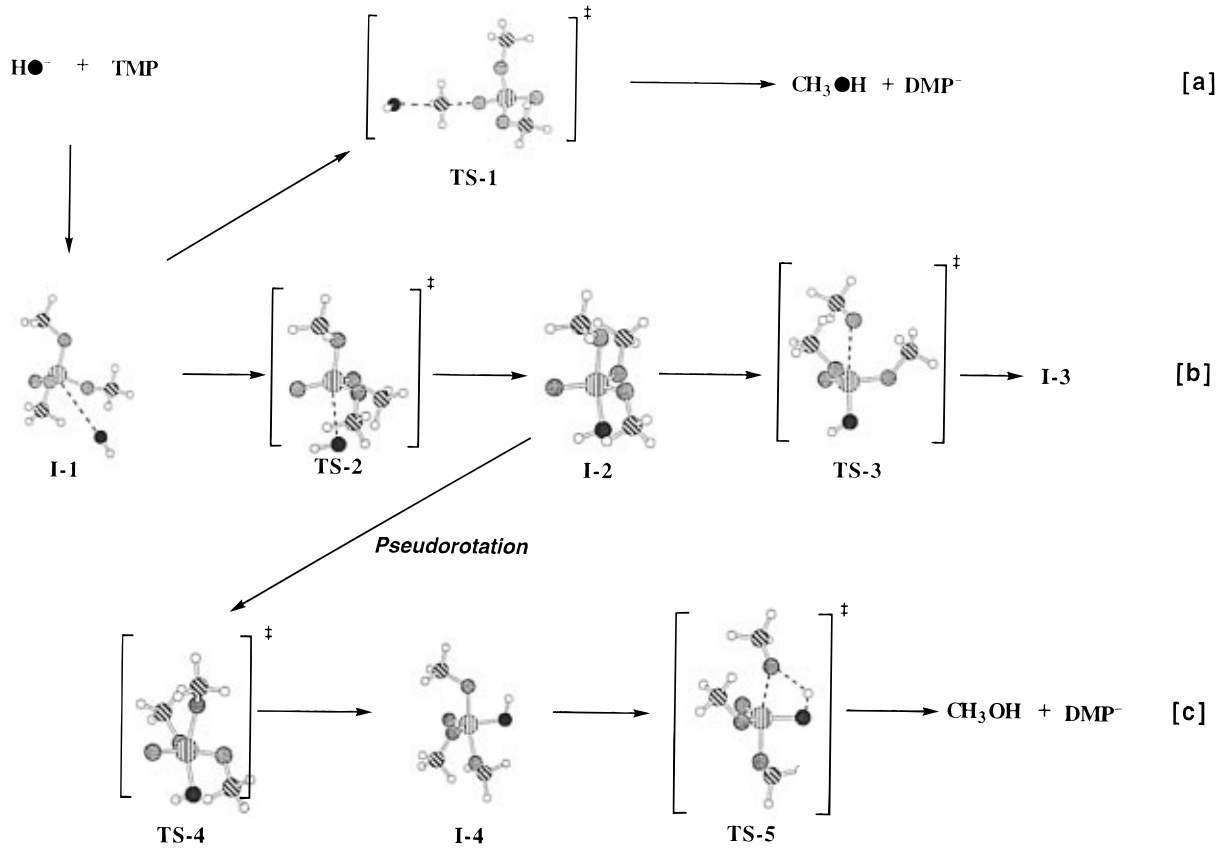

[a] Not all transition states and intermediates along all three pathways are depicted for the sake of clarity. **I-2** and **I-4** have the lowest energy among their rotamers (see Figure 4 and Table 2). **I-3** corresponds to the ion−dipole complex, $(CH_3O)^-...(HO)(CH_3O)_2PO$, which can further undergo reactions as described in text. The black oxygen denotes ^{18}O-labeled $(OH)^-$.

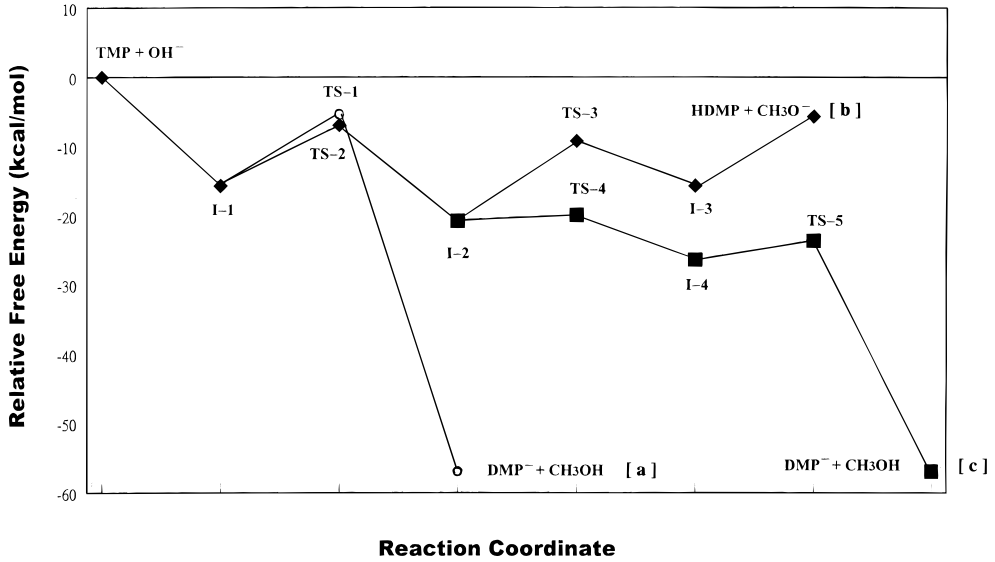

Figure 1. Relative MP2/6-31+G*//HF/6-31+G* activation free energies for the gas-phase reaction of $(OH)^-$ with TMP. The zero of energy corresponds to the reactants at infinite separation. The free energy of **I-3**, which was not computed, was assumed to be similar to that of **I-1**. Note that pathways a and c lead to the same set of products, which have been displaced in the reaction coordinate diagram for the sake of clarity.

calculated activation free energies indicate that an *adjacent* mechanism (pathway c) is kinetically more favorable than an *in-line* mechanism (where entering and leaving groups are "in-line") since both **TS-4** and **TS-5** are lower in free energies than **TS-3** (by 10.7 and 14.4 kcal/mol, Table 2 and Figure 1); i.e., there is no significant barrier to pseudorotation and in contrast to **TS-3**, **TS-5** is stabilized by favorable electrostatic interactions between the hydroxyl hydrogen and the departing oxygen, as evidenced by MP2/6-31+G* CHelp[19] partial atomic charges of −0.72 on the departing oxygen, 0.25 on the hydroxyl proton, and a distance of 1.78 Å between them.

The rate-limiting transition states for the reaction of $(OH)^-$ at carbon and phosphorus of TMP are **TS-1** and **TS-2**, respectively. Since the products of pathways a and c are identical and **TS-2** is only slightly lower in free energy than **TS-1** (by 1.6 kcal/mol at MP2/6-31+G*//HF/6-31+G*), nucleophilic substitution at phosphorus is predicted to be kinetically competitive with S_N2 reaction at carbon (Figure 1).

SCHEME 2: Computed $(CH_3O)^-$ + TMP Reaction Pathways Occurring at Carbon (Pathway d) and at Phosphorus (Pathway c)[a]

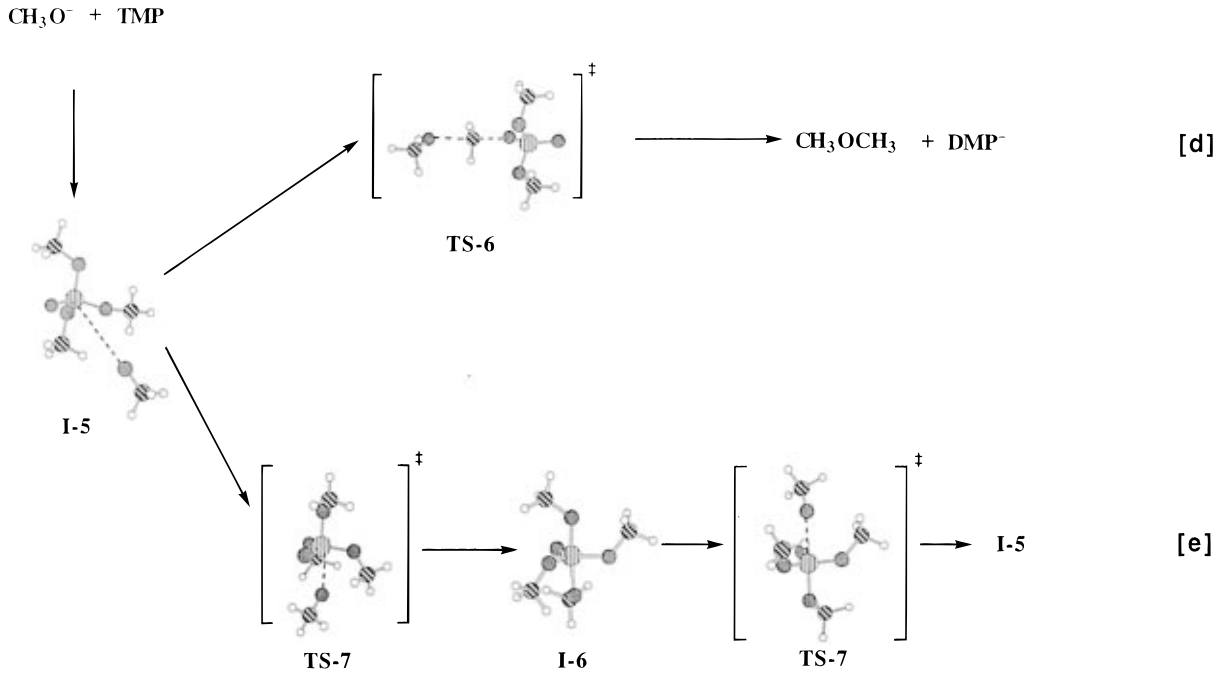

[a] Not all transition states and intermediates along both pathways are depicted for the sake of clarity. **I-5** can further undergo reactions as described in text.

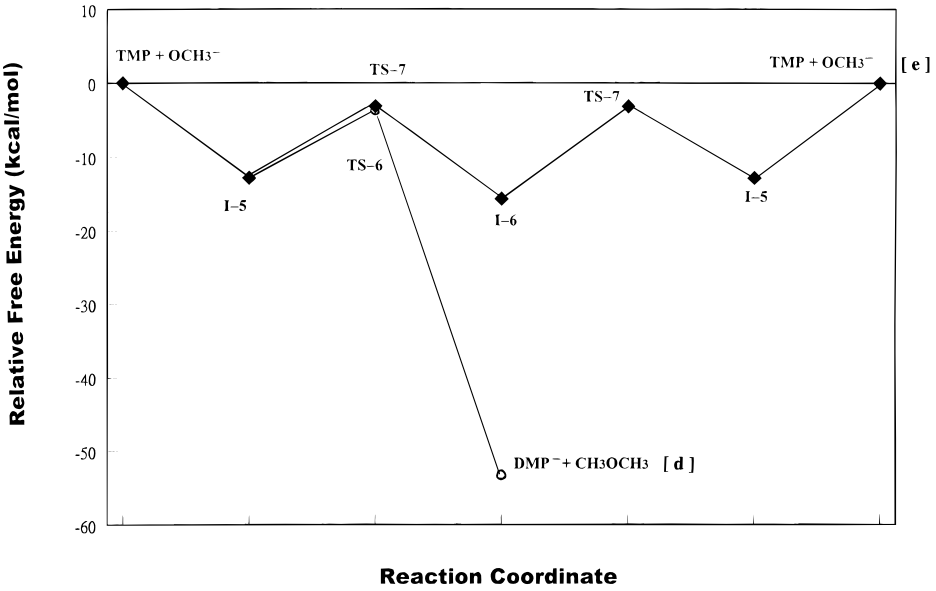

Figure 2. Relative MP2/6-31+G*//HF/6-31+G* activation free energies for the gas-phase reaction of $(CH_3O)^-$ with TMP. The zero of energy corresponds to the reactants at infinite separation.

CH_3O^- + TMP. In Scheme 2, pathway d is S_N2 reaction at carbon via transition state (**TS-6**) to yield CH_3OCH_3 and $(DMP)^-$; the reaction is exothermic with a free energy of −53 kcal/mol. Pathway e is nucleophilic substitution at phosphorus via a long-range transition state (**TS-7**) to form a pentacovalent TBP intermediate (**I-6**). The latter can undergo an isoidentity reaction to yield an ion−dipole complex (**I-5**), which can break down to give $(CH_3O)^-$ and TMP. Alternatively, the methoxide within the ion−dipole complex (**I-5**) can react at carbon to give CH_3OCH_3 and $(DMP)^-$. Since the latter products are thermodynamically much more stable than the products from the thermoneutral reaction, the fate of **I-5** will be dominated by S_N2 reaction at carbon; hence pathways d and e are expected to yield the same products, CH_3OCH_3 and $(DMP)^-$. Nucleophilic addition of $(CH_3O)^-$ to TMP followed by pseudorotation will generate products that are identical to those of an in-line mechanism.

As for gas-phase reaction of $(OH)^-$ with TMP, the rate-limiting transition state for the reaction of $(CH_3O)^-$ at carbon, **TS-6**, is higher in *energy* (by 5.6 kcal/mol) than that at phosphorus, **TS-7** (Table 2). However, inclusion of ZPE, vibrational energy, and entropy results in a slightly lower *free* energy for **TS-6** relative to **TS-7**. Since the free energy difference between the two transition states is only 0.5 kcal/mol (see Table 2 and Figure 2), pathways d and e are both competitive channels.

F^- + TMP. In Scheme 3, an adjacent mechanism was not considered since pseudorotation of **I-8** will place the electrone-

SCHEME 3: Computed F^- + TMP Reaction Pathways Occurring at Carbon (Pathway f) and at Phosphorus (Pathway g)[a]

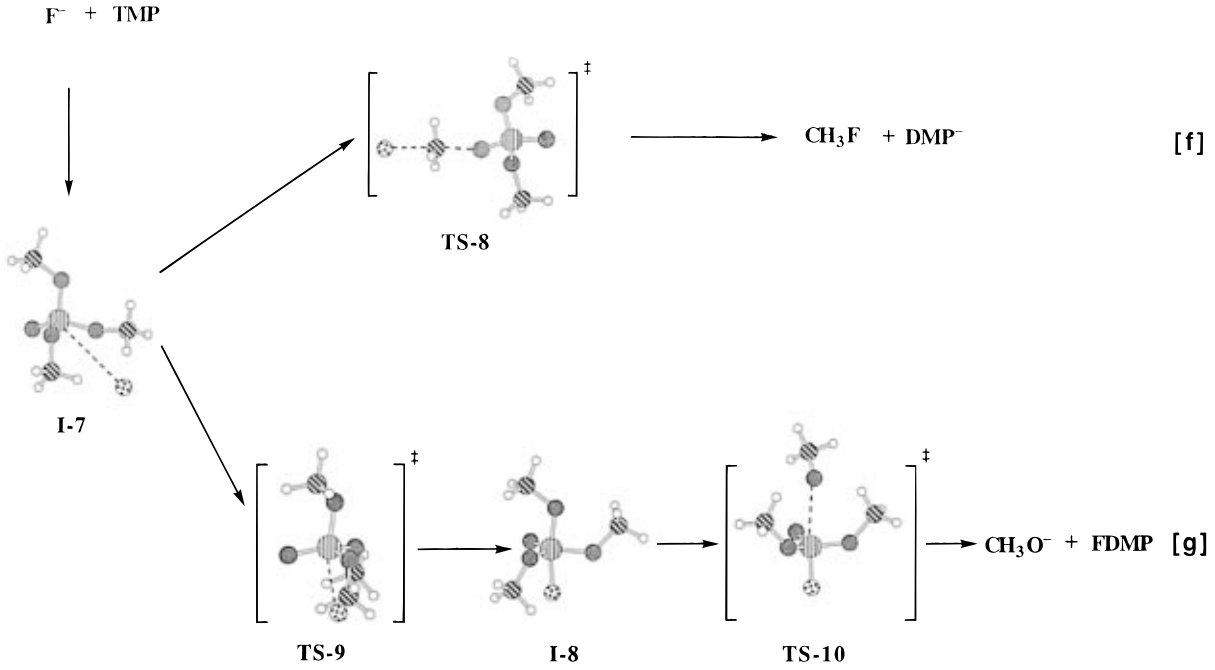

[a] Not all transition states and intermediates along both pathways are depicted for the sake of clarity. FDMP is $(F)(CH_3O)_2PO$.

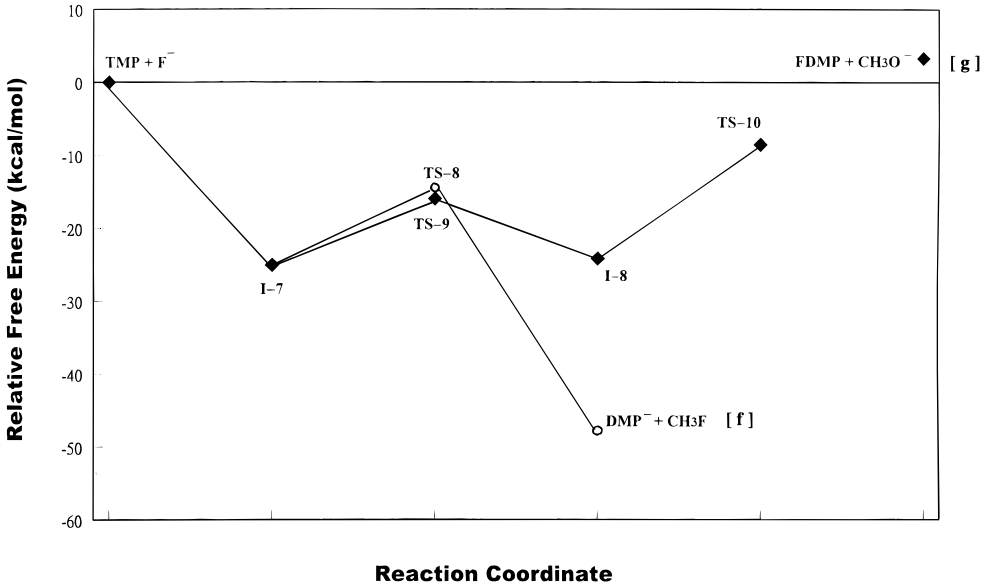

Figure 3. Relative MP2/6-31+G*//HF/3-21+G* activation free energies for the gas-phase reaction of F^- with TMP. The zero of energy corresponds to the reactants at infinite separation. The **TS-10** transition state is expected to yield a $CH_3O^-...(CH_3O)_2PO(F)$ intermediate, which has not been computed.

gative F atom in an unfavorable equatorial position. In contrast to $(OH)^-$ reaction at TMP(P), the transition state for methoxide elimination, **TS-10**, is significantly higher in free energy (by 7.4 kcal/mol at MP2/6-31+G*//HF/3-21+G*, Table 2) than that for fluoride addition, **TS-9**; thus, for the reaction of F^- with TMP, the rate-limiting step for nucleophilic substitution at phosphorus is $(CH_3O)^-$ elimination. Since the rate-limiting transition state for reaction at phosphorus, **TS-10**, is higher in free energy than that for reaction at carbon, **TS-8** (by 5.9 kcal/mol at MP2/6-31+G*//HF/3-21+G*, Table 2), S_N2 reaction at carbon is kinetically favored over nucleophilic substitution at phosphorus (Figure 3). The former (pathway f) is also thermodynamically favored over the latter (pathway g).

Discussion

Assessment of Errors. The activation free energies based on the MP2/6-31+G*//HF/6-31+G* calculations (see Results) predict that nucleophilic substitution at phosphorus competes with S_N2 reaction at carbon for $(OH)^-$ and $(CH_3O)^-$ attack of TMP. To determine the reliability of the MP2/6-31+G*//HF/6-31+G* results, additional calculations were performed to evaluate the dependence of the MP2/6-31+G*//HF/6-31+G* results for $(OH)^-$ and $(CH_3O)^-$ attack of TMP on (i) the geometry optimization protocol, (ii) the size of the basis sets, and (iii) the level of theory used to estimate electron correlation. The geometries of the rate-limiting transition states for the reaction of $(OH)^-$ and $(CH_3O)^-$ at the carbon and phosphorus sites of TMP were reoptimized at the MP2/6-31+G* level. Two

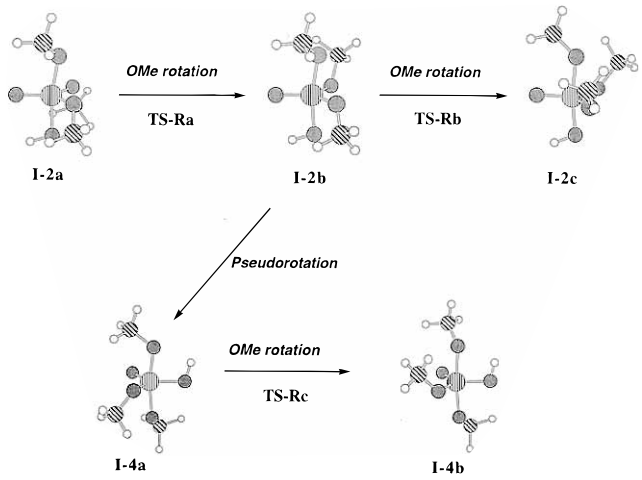

Figure 4. TMP−$(OH)^-$ TBP conformers.

TABLE 3: Dependence on Geometry Optimization Level, Basis Set Size, and Treatment of Electron Correlation

theory level	E(TS−P)[c]	E(TS−C)[d]	ΔE[e]	ΔG[f]
	OH^- + TMP			
MP2/6-31+G*[a]	−835.949 00	−835.938 17	6.79	1.58
MP2/6-31+G*[b]	−835.957 63	−835.946 26	7.14	1.93
MP2/6-311++G(3df,3pd)[b]	−836.664 64	−836.653 79	6.80	1.59
MP4(SDQ)/6-31+G*[b]	−836.010 89	−835.999 94	6.87	1.66
	CH_3O^- + TMP			
MP2/6-31+G*[a]	−875.102 65	−875.093 68	5.63	−0.46
MP2/6-31+G*[b]	−875.110 58	−875.102 26	5.22	−0.87
MP2/6-31++G(3df,3pd)[b]	−875.869 30	−875.961 01	5.20	−0.89
MP4(SDQ)/6-31+G*[b]	−875.176 98	−875.168 80	5.13	−0.96

[a] Geometries optimized at the HF/6-31+G* level. [b] Geometries optimized at the MP2/6-31+G* level. [c] Energy of the rate-limiting transition state for reaction at phosphorus. [d] Energy of the rate-limiting transition state for reaction at carbon. [e] $\Delta E = E$(TS-C) − E(TS-P). [f] Assuming ZPE, E_{TRV}, and S_{TRV} differences listed in Table 2.

single-point calculations were carried out at the MP2/6-311++G(3df,3pd) and MP4(SDQ)/6-31+G* levels using the MP2/6-31+G* optimized geometries. The results are summarized in Table 3.

For the $(OH)^-$ + TMP reaction, the energy difference, E(**TS-1**) − E(**TS-2**), is 6.79, 7.14, 6.80, and 6.87 kcal/mol at the MP2/6-31+G*//HF/6-31+G*, MP2/6-31+G*//MP2/6-31+G*, MP2/6-311++G(3df,3pd), and MP4(SDQ)/6-31+G* levels of theory, respectively. All three sets of calculations at higher levels of theory predict a larger positive energy difference, E(**TS-1**) − E(**TS-2**), relative to the MP2/6-31+G*//HF/6-31+G* value (by 0.01−0.35 kcal/mol). Assuming similar enthalpic and entropic corrections to those obtained in Table 2, the activation free energy difference between **TS-1** and **TS-2** based on the MP4(SDQ)/6-31+G* energies is 1.7 kcal/mol. This verifies the prediction that nucleophilic substitution at phosphorus is competitive and slightly more favorable than S_N2 reaction at carbon.

For the $(CH_3O)^-$ + TMP reaction, the energy difference, E(**TS-6**) − E(**TS-7**), is 5.63, 5.22, 5.20, and 5.13 kcal/mol at the MP2/6-31+G*//HF/6-31+G*, MP2/6-31+G*//MP2/6-31+G*, MP2/6-311++G(3df,3pd), and MP4(SDQ)/6-31+G* levels of theory, respectively. Thus, increasing the level of theory decreases the energy difference, E(**TS-6**) − E(**TS-7**), so that inclusion of the vibrational energy and entropy in Table 2 results in a lower activation *free* energy for **TS-6** relative to **TS-7** (by −0.96 kcal/mol at MP2(SDQ)/6-31+G*). This verifies the prediction (see Results) that $(CH_3O)^-$ reacts at both the carbon and phosphorus sites of TMP although nucleophilic substitution at carbon is slightly favored kinetically over that at phosphorus, in contrast to the gas-phase reaction of $(OH)^-$ with TMP.

In the ensuing discussion, our conclusions are based on *relative* rather than "absolute" energy or free energy differences. For example, in elucidating the factors governing the site of reactivity of a given nucleophile toward TMP, the rate-limiting transition state for S_N2 reaction at carbon is compared with that for nucleophilic substitution at phosphorus. Any systematic errors in the relative gas-phase free energies (arising from the basis set employed and treatment of electron correlation) are likely to cancel. Hence, emphasis is placed on relative free energy differences (as opposed to "absolute" values) in interpreting the results (see below).

Effects of Conformational Entropy. Apart from a loss in translational, rotational, and vibrational entropy upon addition of a nucleophile to TMP, there is also a conformational entropy loss in going from the ground state to the rate-limiting transition state. This is because in the ground state the three methoxyl groups in TMP are free to rotate about their respective P−O bonds, whereas in the transition state the rotation of at least one of the methoxyl groups becomes restricted.

In the case of $(OH)^-$ and $(CH_3O)^-$ attack of TMP, the conformational entropy difference between the rate-limiting transition states for nucleophilic substitution at carbon and at phosphorus can be estimated from

$$S_{conf} = -R\sum_i p_i \ln p_i \qquad (3)$$

where p_i, the fractional population of each rotamer state i, is given by

$$p_i = \frac{\exp(-E_i/RT)}{\sum_i \exp(-E_i/RT)} \qquad (4)$$

R is the gas constant, T is the temperature, and E_i is the energy of rotamer i. Since the three carbon and three methoxy oxygen atoms are indistinguishable, a nucleophile can attack at each of the three carbon atoms giving rise to three isomeric TS-C (**TS-1** or **TS-6**) transition states. Similarly, it can attack the phosphorus atom resulting in three isomeric TS-P (**TS-2** or **TS-7**) transition states with each of three methoxy oxygen atoms in the axial position.

In the rate-limiting transition state for reaction at phosphorus (**TS-2** or **TS-7**), the two equatorial methoxyl groups are constrained in the "down" conformation with the methyl groups pointing toward the anion in order to minimize electrostatic repulsion between the incoming nucleophile and the negative charge equatorial oxygens; no transition state with different orientations of the equatorial methoxy groups could be found. Only the methoxyl group in the axial position can undergo rotation about the axial P−O bond to yield three isomeric transition states with the axial C−O bond either gauche, trans, or -gauche with respect to the equatorial P═O bond. Thus, there is a total of $3 \times 3 = 9$ transition state isomers. In the rate-limiting transition state for S_N2 reaction at carbon (**TS-1** or **TS-6**), the methoxyl group involved in bond formation with the nucleophile is constrained whereas each of the other two methoxyl groups has three local rotational minima, yielding a total of $3 \times 3 \times 3 = 27$ transition state rotamers.

Assuming that each rotamer is populated equally, an *upper* bound of the conformational entropy difference between the carbon and phosphorus rate-limiting transition states is estimated from eqs 3 and 4 to be $-R[(27 \times {}^1/_{27} \ln {}^1/_{27}) - (9 \times {}^1/_9 \ln {}^1/_9)] = 2.2$ cal/mol/K. Thus $T\Delta S_{conf} = 0.65$ kcal/mol at 298 K; the actual value will be less than 0.65 kcal/mol since the various isomers are likely to differ in energy. Thus qualitatively, the effect of conformational entropy is to bias the attack toward

TABLE 4: Enthalpic vs Entropic Factors Governing Site Reactivity[a]

anion	ΔE	ΔZPE	ΔE_{TRV}	ΔH	$T\Delta S_{TRV}$	$T\Delta S_{conf}$	ΔG
$(OH)^-$	6.87	−1.53	−0.70	4.64	2.98	0.65	1.01
$(CH_3O)^-$	5.13	−1.49	−0.67	2.97	3.96	0.65	−1.61

[a] Differences in activation energies and entropies (in kcal/mol) of the rate-limiting transition states for reaction at carbon and phosphorus. The ΔE are MP4(SDQ)/6-31+G* values taken from Table 3. ΔZPE, ΔE_{TRV}, and $T\Delta S_{TRV}$ are taken from Table 2. See text for estimation of $T\Delta S_{conf}$. $\Delta H = \Delta E + \Delta ZPE + \Delta E_{TRV}$. $\Delta G = \Delta H - T\Delta S_{TRV} - T\Delta S_{conf}$.

TABLE 5: Experimentally Observed Product Distribution for Reaction of Anions with TMP in Vacuum at 298 K[a]

anion	product	% product yield
$(OH)^-$	$(C_2H_6O_4P)^-$	93.1
	$(C_2H_6O_3P)^-$	6.9[b]
$(CH_3O)^-$	$(C_2H_6O_4P)^-$	100
$(CD_3O)^-$	$(C_2H_6O_4P)^-$	98.5
	$(C_2D_3H_3O_4P)^-$	1.5
F^-	$(C_2H_6O_4P)^-$	100

[a] Data taken from *J. Am. Chem. Soc.* **1992**, *114*, 8622, Table I. [b] This product results from elimination across a C−O bond at carbon, a pathway that has not been considered in this work.

the carbon site; quantitatively, inclusion of the $T\Delta S_{conf}$ estimate of 0.65 kcal/mol to the relative MP4(SDQ)/6-31+G* energies in Table 3 and the relative enthalpy and entropy values in Table 2 yields a free energy difference, G(**TS-1**) − G(**TS-2**), of 1.0 kcal/mol and G(**TS-7**) − G(**TS-6**) of 1.6 kcal/mol (Table 4). Thus, taking into account the (quantitative) effects of conformational entropy does not appear to change our key finding that nucleophilic substitution at phosphorus can effectively compete with S_N2 reaction at carbon for the gas-phase reaction of $(OH)^-$ with TMP.

Comparison with Experiment. Table 5 summarizes the distribution of experimentally observed product ions for the reactions of the three nucleophiles studied here ($(OH)^-$, $(CH_3O)^-$, and F^-) with TMP in the gas phase at 298 K. The TMP + $(CH_3O)^-$ reaction profile in Figure 2 shows that phosphorus attack is kinetically competitive with carbon attack. However, $(DMP)^-$, a product of the carbon attack channel, is a far better leaving group than $(CH_3O)^-$, a product of the phosphorus attack pathway, as evidenced by a significantly lower reaction free energy relative to the thermoneutral identity reaction (Table 2). Thus, the methoxide within the ion−dipole complex (**I-5**) will likely react at carbon again to yield the more stable products, CH_3OCH_3 and $(DMP)^-$ (see also Results). Consequently, the reaction of $(CH_3O)^-$ with TMP will yield predominantly S_N2(C) nucleophilic substitution products as the reaction proceeds to equilibrium; this is consistent with the observation of 100% $((CH_3O)_2PO_2)^-$ for the TMP + $(CH_3O)^-$ reaction (Table 5). The prediction that there are two kinetically competitive pathways, nucleophilic substitution at phosphorus and at carbon, is supported by the observed product distribution for the TMP + $(CD_3O)^-$ reaction, which resulted in 98.5% $((CH_3O)_2PO_2)^-$ and 1.5% $((CD_3O)(CH_3O)PO_2)^-$. The appearance of $((CD_3O)(CH_3O)PO_2)^-$ can only be explained if $(CD_3O)^-$, besides reacting at carbon, also attacks the phosphorus of TMP yielding a $(CH_3O)^-...(CD_3O)(CH_3O)_2PO$ ion−dipole complex (like **I-5**), and the $(CH_3O)^-$ within this complex subsequently reacts at carbon to form $((CD_3O)(CH_3O)PO_2)^-$, the observed product, and CH_3OCH_3. For the reaction of $(CD_3O)^-$ with TMP, the relative rate for nucleophilic substitution at carbon vs nucleophilic substitution at phosphorus is experimentally estimated to be 43:1.[3] Using transition-state theory, this yields a free energy difference, G(TS-P) − G(TS-C), of 2.2 kcal/mol, which compares well with the corresponding computed value for $(CH_3O)^-$ attack of 1.6 kcal/mol at MP4(SDQ)/6-31+G* including conformational entropy (Table 4).

The TMP + $(OH)^-$ reaction profile in Figure 1 shows that hydroxide reacts with TMP in the gas phase *both* at carbon and phosphorus to yield $(DMP)^-$ and CH_3OH, consistent with the products found experimentally (Table 5). In previous work,[1−3] *intra*molecular proton transfer, as depicted in **TS-5**, was not taken into consideration. Even though Lum and Grabowski considered *inter*molecular proton transfer between the hydroxyl hydrogen and the departing methoxide within the $(CH_3O)^-...(HO)(CH_3O)_2PO$ ion−dipole complex and stated that they "cannot unequivocally distinguish between reaction at the carbon and phosphorus sites since both reactions are expected to yield the same products," they predicted that "predominant reaction at carbon with a tiny amount of reaction at phosphorus seems most likely for $(OH)^-$," based on the observation that $(CD_3O)^-$ gave only 1.5% products resulting from attack at phosphorus of TMP.[3] In contrast, the small (1 kcal/mol) difference in the computed free energies of **TS-1** and **TS-2** suggests roughly equal amounts of reaction at phosphorus and carbon. Specifically, the estimated free energy difference, G(**TS-1**) − G(**TS-2**), of 1 kcal/mol (Table 4) would predict the nucleophilic substitution rate at phosphorus to be roughly five times that at carbon. (Note that the accuracy of the latter relies upon cancellation of systematic errors in the two different types of transition states, see above).

The predicted product distribution for the TMP + F^- gas-phase reaction is also in accord with the experimental product distribution.[2,3] Intramolecular proton transfer cannot take place and methoxide is formed when F^- attacks at the phosphorus of TMP. Since nucleophilic substitution at TMP(P) is both thermodynamically and kinetically unfavorable (Figure 3), $(DMP)^-$ resulting from S_N2 reaction at carbon is predicted to be the only product in the gas-phase reaction of F^- with TMP, in accord with the products seen experimentally (Table 5).

The calculations also predict the absence of methoxide for all three reactions studied here. Thus, our calculations support the results of Lum and Grabowski,[3] who found no methoxide for all anions studied that react with TMP, in contrast to the methoxide observed by Asubiojo and co-workers[1] and Hodges and co-workers.[2]

Factors Controlling the Site of Reactivity (C or P) of TMP in Vacuum. The reaction mechanisms revealed for the reactions studied show that the nature of the nucleophile does not dictate the site of reactivity. This is evident in the case of the F^- + TMP reaction, where the rate-limiting transition state for reaction at phosphorus is not addition of the nucleophile, F^-, but elimination of methoxide. Instead, both thermodynamic and/or kinetic factors control the type of reaction and thus, site of reactivity, as revealed by the present set of calculations.

Thermodynamic Control. In the gas phase, $(DMP)^-$ anion is a better leaving group than $(CH_3O)^-$; thus, the reaction pathway that produces $(DMP)^-$ as product will be thermodynamically favored over that yielding $(CH_3O)^-$ as product. This is the case for the reaction of $(CH_3O)^-$ and F^- with TMP, and, in the latter, the site of reactivity is governed by the reaction thermodynamics: attack at phosphorus does not occur at 298 K since the reaction free energy F^- + TMP → $(CH_3O)^-$ + $(F)(CH_3O)_2PO$ is positive (Table 2). For the reaction of $(OH)^-$ with TMP(P), intramolecular proton transfer plays an important role since its generates $(DMP)^-$ instead of $(CH_3O)^-$ as product, making nucleophilic substitution at phosphorus and at carbon equally favorable from a thermodynamic standpoint. Note that previous work[3] reasoned that attack at phosphorus was insignificant in the gas phase since "if the nucleophile were to attack the phosphorus, it must extrude methoxide as the leaving group."

TABLE 6: Partial Atomic Charges on P and C Atoms of TMP

method	basis set	q(P)	$\langle q(C)\rangle^a$
Mulliken	HF/6-311++G(3df,3pd)	1.3	0.5
Mulliken	MP2/6-31+G*	2.1	−0.4
NBO	MP2/6-31+G*	2.6	−0.3
CHELP	MP2/6-31+G*	1.7	0.5
CHELPG	MP2/6-31+G*	1.2	0.1

[a] Charge averaged over the three methoxy carbon atoms.

Kinetic Control. In contrast to the F^- + TMP reaction, the site of reactivity for $(CH_3O)^-$ and $(OH)^-$ attack of TMP is kinetically controlled and the rate-limiting barrier for the reaction of $(CH_3O)^-$ or $(OH)^-$ at TMP(P) is nucleophilic addition rather than elimination (or pseudorotation/OMe rotation). Table 4 shows that both enthalpic and entropic terms contribute to the relative reactivity of nucleophilic substitution at phosphorus vs S_N2 reaction at carbon. For the $(OH)^-$ and $(CH_3O)^-$ reactions with TMP, $\Delta E(0\ \mathrm{K}) = E(\mathrm{TS\text{-}C}) - E(\mathrm{TS\text{-}P})$ is positive, indicating that anion attack at phosphorus is favored over carbon. Since ZPE favors formation of the "looser" TS-C transition state, the dominant force favoring attack at phosphorus is electrostatic, stemming from the more electropositive character of the phosphorus site relative to the carbon one in TMP as evidenced by a significantly smaller average partial atomic charge on the carbon atoms compared to phosphorus (Table 6). However, the thermal corrections arising from vibrational energy, vibrational entropy, and conformational entropy all favor S_N2 reaction at carbon.

Thus, for anion reactions with TMP(P) where the rate-limiting step is nucleophilic addition of TMP(P) rather than elimination or pseudorotation, there are essentially two factors that control the site of reactivity: Temperature-independent electrostatic factors favor attack at phosphorus, whereas temperature-dependent entropic factors bias the attack toward carbon. At very low temperatures, the reaction of $(CH_3O)^-$ and $(OH)^-$ at phosphorus is predicted to be kinetically more favorable than that at carbon, whereas the converse is true at high temperatures where entropic effects become dominant. Note that this correlates with the observation that the mechanism for alkaline hydrolysis of TMP in solution changes from reaction at phosphorus to reaction at carbon at high temperatures.[6]

Conclusions

In summary, the present calculations suggest two key novel features that can be tested experimentally. First, the experimentally observed $(DMP)^-$ resulting from $(OH)^-$ attack of TMP is generated *not only* from a S_N2 reaction at carbon (pathway a) but also from an addition−pseudorotation−elimination−intramolecular proton transfer reaction at phosphorus (pathway c). The predicted reaction of $(OH)^-$ at phosphorus (in addition to carbon) can be verified by performing an ^{18}O-labeled $(OH)^-$ experiment and observing ^{18}O-enriched $(DMP)^-$ with retention of configuration (Scheme 1). Such ^{18}O-labeled $(OH)^-$ experiments had been planned by Lum and Grabowski to confirm their expectation that hydroxide reacts predominantly at carbon with a tiny amount of reaction at phosphorus, but no results have been published to date (to our knowledge). Thus, for $(OH)^-$ attack of TMP at 298 K, if nucleophilic substitution at phosphorus occurs in addition to S_N2 reaction at carbon, then ^{18}O-enriched and non-^{18}O-enriched $(DMP)^-$ would be observed. Second, vibrational entropy and, to a lesser extent, vibrational energy influence the site of reactivity. This can be tested experimentally by performing ^{18}O-labeled $(OH)^-$ and $(CH_3O)^-$ temperature-dependent experiments. For example, in an $^{18}(OH)^-$ reaction with TMP, the amount of ^{18}O-enriched $(DMP)^-$ would increase with decreasing temperature such that ^{18}O-enriched $(DMP)^-$ would be the major product at temperatures ≤ 298 K.

Acknowledgment. N.Y.C. is supported by the Institute of Biomedical Sciences, Academia Sinica, Taiwan. This work was supported by the Institute of Biomedical Sciences, Academia Sinica, Academia Sinica Computing Center, the National Center for High Performance Computing in Taiwan, and the National Science Council, Taiwan.

References and Notes

(1) Asubiojo, O. I.; Brauman, J. I.; Levin, R. H. *J. Am. Chem. Soc.* **1997**, *99*, 7707−7708.
(2) Hodges, R. V.; Sullivan, S. A.; Beauchamp, J. L. *J. Am. Chem. Soc.* **1980**, *102*, 935−938.
(3) Lum, R. C.; Grabowski, J. J. *J. Am. Chem. Soc.* **1992**, *114*, 8619−8627.
(4) Blumenthal, E.; Herbert, J. B. M. *Trans. Faraday Soc.* **1945**, *41*, 611−617.
(5) Barnard, P. W. C.; Bunton, C. A.; Llewellyn, D. R.; Vernon, C. A.; Welch, V. A. *J. Chem. Soc.* **1961**, 2670−2676.
(6) Hudson, R. F. In *Structure and* Mechanism *in Organophosphorus Chemistry*; Academic Press: New York, 1965.
(7) Westheimer, F. H.; Huang, S.; Covitz, F. *J. Am. Chem. Soc.* **1988**, *110*, 181−185.
(8) Baran, J.; Penczek, S. *Macromolecules* **1995**, *28*, 5167−5176.
(9) Thatcher, G. R. J.; Kluger, R. *Adv. Phys. Org. Chem.* **1989**, *25*, 99.
(10) Lim, C.; Tole, P. *J. Phys. Chem.* **1992**, *96*, 5217−5219.
(11) Tole, P.; Lim, C. *J. Phys. Chem.* **1993**, *97*, 6212−6219.
(12) Lim, C.; Tole, P. *J. Am. Chem. Soc.* **1992**, *114*, 7245−7252.
(13) Frisch, M. J.; Trucks, G. W.; Schlegel, H. B.; Gill, P. M. W.; Johnson, B. G.; Robb, M. A.; Cheeseman, J. R.; Petersson, T.; Keith, G. A.; Montgomery, J. A.; Raghavachari, K.; Al-Laham, M. A.; Zakrzewski, V. G.; Ortiz, J. V.; Foresman, J. B.; Cioslowski, J.; Stefanov, B. B.; Nanayakkara, A.; Challacombe, M.; Peng, C. Y.; Ayala, P. Y.; Chen, W.; Wong, M. W.; Andres, J. L.; Replogle, E. S.; Gomperts, R.; Martin, R. L.; Fox, D. J.; Binkley, J. S.; Defrees, D. J.; Baker, J.; Stewart, J. P.; Head-Gordon, M.; Gonzalez, C.; Pople, J. A. In *Gaussian 94*; Gaussian Inc.: Pittsburgh, PA, 1995.
(14) Fukui, K. *Acc. Chem. Res.* **1981**, *14*, 363−368.
(15) Gonzalez, C.; Schegel, H. B. *J. Chem. Phys.* **1989**, *90*, 2154−2161.
(16) Gonzalez, C.; Schegel, H. B. *J. Phys. Chem.* **1990**, *94*, 5523−5527.
(17) Hehre, W. J.; Radom, L.; Schleyer, P. v. R.; Pople, J. A. *Ab Initio Molecular Orbital Theory*; John Wiley and Sons: New York, 1986.
(18) McQuarrie, D. A. *Statistical Mechanics*; Harper and Row: New York, 1976.
(19) Chirlian, L. E.; Francl, M. M. *J. Comput. Chem.* **1987**, *8*, 894.